
1 This manuscript is a preprint and will be submitted for publication in *Scientific report*. Please
2 note that, despite having undergone peer-review, the manuscript has not yet been accepted for
3 publication. Subsequent versions of this manuscript may have slightly different content. If
4 accepted the final version of this manuscript will be available via the '*Peer-reviewed*
5 *Publication DIO*' link on the right-hand side of this webpage. Please feel free to contact any
6 of the authors; we welcome feedback.

7 Bedload transport in rivers: size matters but so does shape!

8 **Cassel Mathieu*¹, Lavé Jérôme², Recking Alain³, Malavoi Jean-René⁵ and Piégay Hervé¹**

9 *¹ University of Lyon, CNRS UMR 5600 Environnement Ville et Société, Site ENS de Lyon, 15*
10 *Parvis René Descartes, BP 000F-69342 Lyon Cedex 07, France. casselmathieu@gmail.com*
11 *and herve.piegay@ens-lyon.fr*

12 *³ CRPG-CNRS, CRPG, Vandœuvre-lès-Nancy, 15, rue Notre Dame des Pauvres BP 20, 54500*
13 *Vandœuvre les Nancy, France. jlave@crpg.cnrs-nancy.fr*

14 *⁴ Inrae, UR ETNA, Domaine Universitaire, 2 rue de la papeterie BP 76, 38402 Saint-Martin-*
15 *d'Hères, France. alain.recking@inrae.fr*

16 *⁵ Electricité De France - EDF/DPIH, Département Concessions Eau Environnement*
17 *Territoires. Le PRIMAT - 190 rue Garibaldi, 69003 LYON, France. jean-rene.malavoi@edf.fr*

18

19 **ABSTRACT**

20 Bedload transport modelling in rivers, which defines the threshold for pebble movement, takes
21 into account the size and density of pebbles, but does not formally consider particle shape. The
22 lack of analyses evaluating the influences of shape and density on particle mobility presents a
23 major deficiency. To address this issue and to compare the relative roles of the density and
24 shape of particles, we performed original sediment transport experiments in an annular flume
25 using molded artificial pebbles equipped with a radio frequency identification tracking system.
26 The particles were designed with four distinct shapes and four different densities while having
27 the same volume, and their speeds and distances traveled under constant hydraulic conditions
28 were analyzed. The results show that particle shape has more influence than particle density on
29 the resting time between particle displacement and the mean traveling distance. For all densities
30 investigated, the particle shape systematically induced differences in travel distance that were
31 strongly correlated ($R^2 = 0.94$) with the Sneed and Folks shape index. Such shape influences,

32 although often mentioned, are here quantified for the first time, demonstrating why and how
33 they can be included in bedload transport models.

34

35 INTRODUCTION

36 Sediment transport is a key process in fluvial geomorphology, being important for
37 sustainable management of navigable channels, designing engineering projects, predicting
38 morphological changes and associated hydraulic risks, interpreting sedimentary archives and
39 restoring rivers ¹. It involves three phases of particle mobility: (1) entrainment ²⁻⁶; (2) motion
40 ⁷⁻⁹; and (3) deposition ^{10,11}. Sediment transport at the particle scale is a stochastic phenomenon
41 ^{7,12,8,13,14,9}, which mostly arises from the complex interactions between particle collisions and
42 highly variable friction, drag, and lift forces due to fluid turbulence. Thus, for practical
43 considerations, empirically calibrated sediment transport functions widely use Shields stress
44 number (τ^* or θ) to quantify the balance of the forces exerted on the channel bed particles, and
45 the critical Shields number (τ^*_c), which is the threshold value necessary to set particles in
46 motion, to determine the moments at which drag forces exceed stabilizing forces ($\tau^* > \tau^*_c$) and
47 particles can be entrained ¹⁵⁻²¹. Such approaches have been used to estimate particle stabilizing
48 forces from median pebble size and submerged density ¹⁶. At the river reach scale, sediment
49 transport estimates generally encapsulate a relation depending on the Shields stress, and
50 therefore also include the median grain size ^{20,22-27} of the transported sediment.

51 Published bedload transport datasets from rivers with similar flow conditions,
52 morphologies, and median grain sizes, may show different transport rates, with large variations
53 in the threshold for setting particles in motion ²⁸, variations that can be up to 10-fold ²⁹ around
54 the mean empirical Shields curve ³⁰⁻³². To explain such dispersion, many studies have focused
55 on the role of mixed grain size, hiding effects ³³⁻³⁶, macro-roughness, channel steepness, or bed
56 roughness relative to channel depth ³⁷. However, fewer studies have qualitatively related pebble

57 shape to bedload transport through the influence of pebble angularity^{38,39}, pebble imbrication
58^{34,35,40}, or bed roughness^{34,40,41} (i.e. the D/K ratio, where D is the diameter of the particles to be
59 moved and K is the bed-particle diameter). In environments with smooth-beds ($D > K$) and
60 during low to moderate flood events, coarse particles of spherical or ellipsoid shape were
61 observed⁴² to be more likely to experience entrainment and transport than flatter shapes.
62 Conversely, in rough-bed rivers ($D < K$), Demir and Walsh¹ found that displacement of flatter
63 shapes (i.e. discs and blades) seems to be promoted. Overall, selective shape entrainment and
64 travel length both decrease as flood magnitude increases and/or particle size decreases⁴³.
65 Whereas these previous studies have emphasized that robust deterministic expression of initial
66 motion should encapsulate the role of particle shape and bed roughness in particle motion
67 modelling^{38,39,44,45}, the scarcity of field and experimental data has prevented a quantitative
68 account of this role.

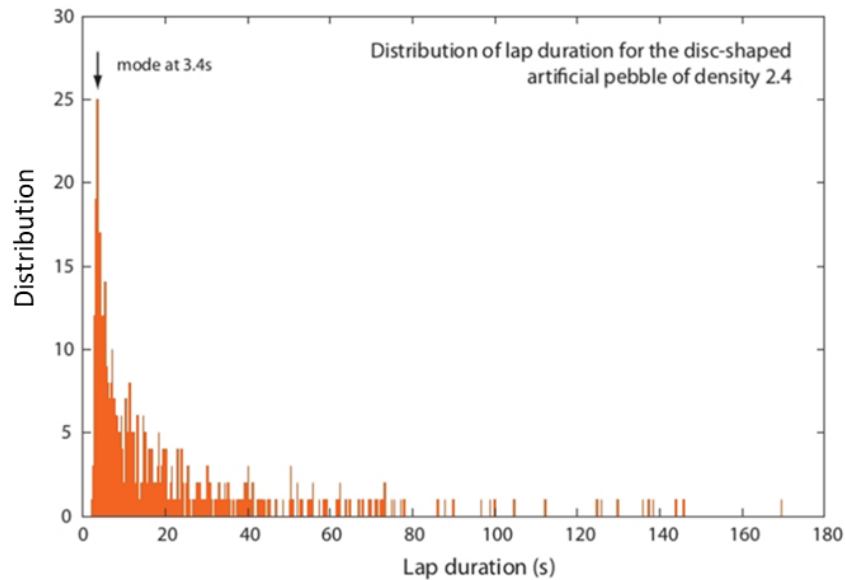
69 To partially fill this gap, we designed a parametric study based on experiments run in
70 an annular flume in which the displacements (encapsulating onset motion, travel length and rest
71 periods) of artificial pebbles of various shapes and densities were tracked for several hours.
72 Particle shape has been quantified by many different parametrizations^{46–52} expressing
73 angularity, surface roughness, or departure from sphericity. As the latter directly impacts on
74 inertial moments and pivoting angle, we investigated the influence of shape in terms of the
75 departure from sphericity, examining various ellipsoid particle shapes (from plate to blade
76 types).

77

78 **RESULTS**

79 The number of revolutions made by the monitored particles ranged between 439 laps
80 for an elongated blade and 2270 laps for a sphere, making the lap duration observations were
81 taken from large sample sizes. Although the lap durations within the annular flume displayed

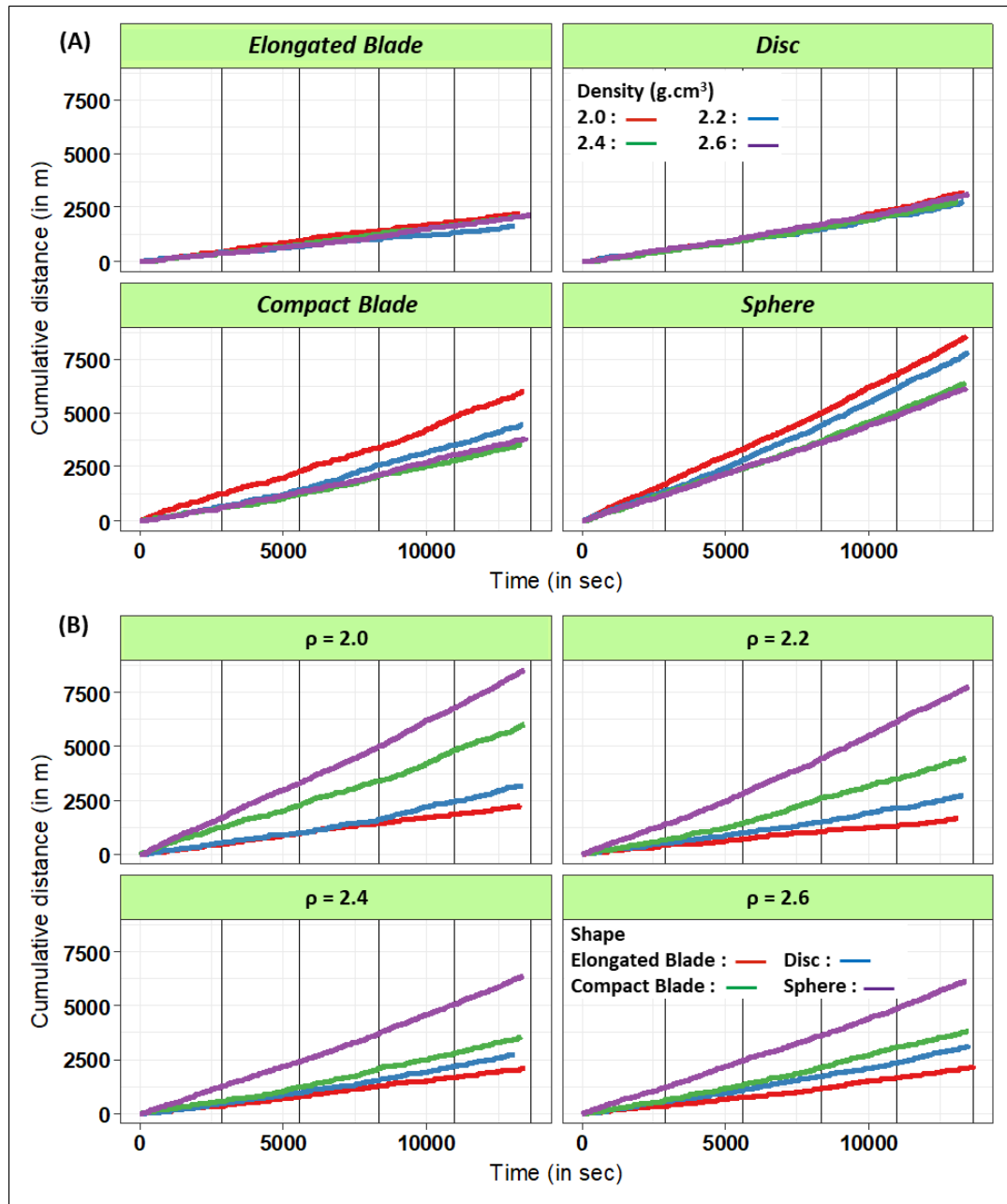
82 large variations (from 3 seconds up to a few minutes; see example in Figure 1) over the total
83 run duration, the cumulative travel distances of the particles (Figure 2) displayed a fairly
84 constant slope that permitted the average traveling velocities of the different artificial pebbles
85 to be defined.



86

87 **Figure 1. Example of the distribution of lap durations (shape = disc; density = 2.4 g.cm⁻³)**

88 The slight increases observed in the slopes of the cumulative distance curves over time
89 for all shapes and densities reflect the progressive augmentation of the particles' velocities
90 caused by a decrease in the mixing load due to abrasion (relative mass loss of 1.2% per
91 kilometer traveled). As this was moderate and affected all tagged particles in a similar manner,
92 we consider that it had very little impact on the first-order estimates and results of the
93 experiments.



94
95 **Figure 2. Cumulative travel distances over time according to particle shape (A) and**
96 **density (B).**

97 The four particle shapes investigated exhibited clear differences in cumulative travel
98 length, with variations in the particle densities also demonstrating effects (Figure 2). The
99 spherical particles traveled the farthest and fastest (mean velocities ranging from 0.44 to 0.60
100 m.s⁻¹), with their mean virtual velocities displaying an inverse relationship with density (Figure
101 3). The compact blade-shaped particles were the second fastest, exhibiting mean velocities
102 ranging from 0.25 to 0.44 m.s⁻¹, again displaying an inverse relationship with density, although

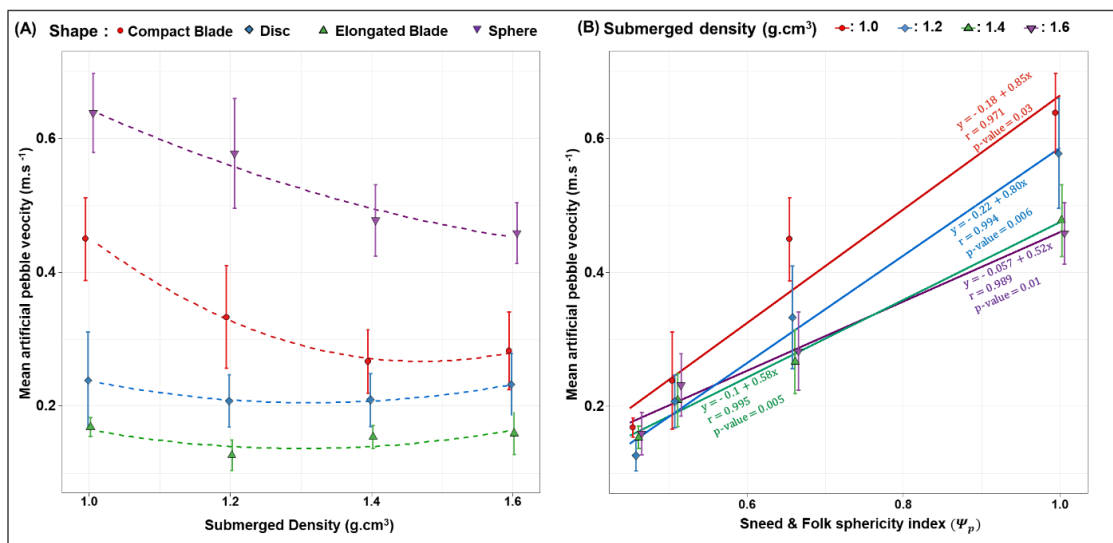
103 to a lesser extent than that of the spherical particles. In contrast, the mean virtual velocities of
 104 the disc- and elongated blade-shaped particles were minimally influenced by their densities: the
 105 mean velocities were clustered within a narrow range from 0.14 to 0.17 m.s⁻¹ and 0.19 to 0.21
 106 m.s⁻¹ respectively. Within the density classes, the distances traveled by the particles clearly
 107 showed a high variability in relation to their shapes (Figure 2B and Figure 3A). The experiments
 108 clearly indicate that the variability in velocity associated with pebble shape is substantially
 109 higher than that associated with particle density (~100% compared with ~30%).

110 To explore the influence of particle shape on mobility in a more quantitative way, we
 111 used the sphericity index, Ψ_p (1), of Sneed and Folks (1958):

$$112 \quad \Psi_p = \sqrt[3]{\frac{S^2}{LI}} \quad \text{Equation (1)}$$

113 where L , I , and S are the longest, intermediate, and shortest axes of the pebbles.

114 The sphericity index Ψ_p shows a remarkable positive relationship with the mean
 115 traveling velocity (Figure 3B). Moreover, the mean velocities increased from 0.52 to 0.85 m.s⁻¹
 116 for decreasing densities from 2.6 to 2.0 g.cm⁻³. These results suggest that it is possible to
 117 estimate differences in the mean virtual velocities and mobilities of particles according to their
 118 sphericity.

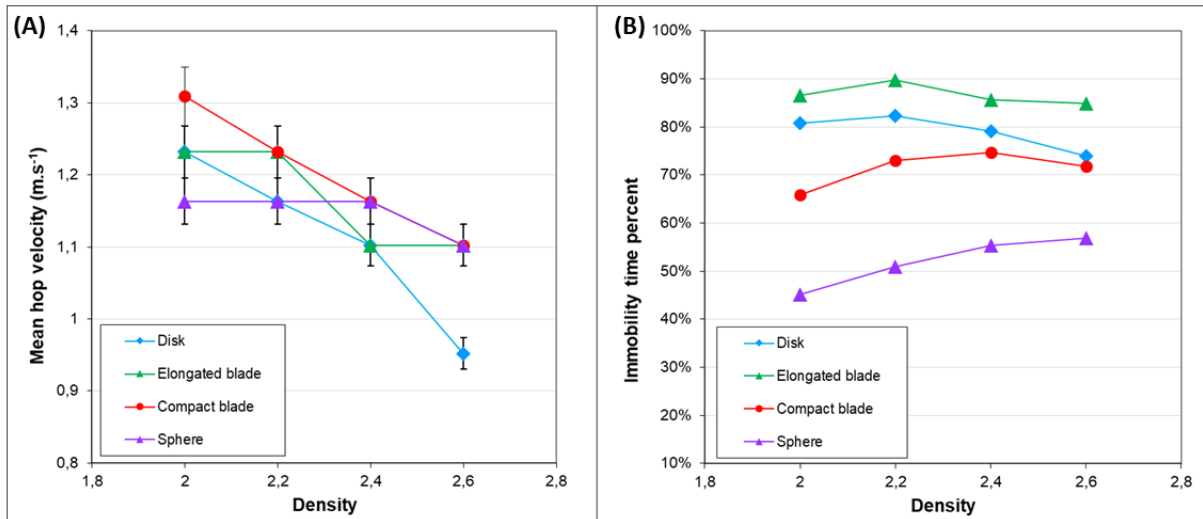


119
 120 **Figure 3. Mean velocity as function of density (A) and Sneed and Folk spherical index (B).**

121 The lap-scaled average travel velocities measured integrate the duration of motion
122 phases and the resting periods in between. However, the pebble shape and density can
123 potentially impact each of these two phases differently. The lap duration distributions are
124 characterized by a first peak at around 3 s in all experiments (Figure 1), which corresponds to
125 a revolution speed of $\sim 1.2 \text{ m.s}^{-1}$. For experimental conditions similar to those used in this study,
126 high speed camera viewing⁵⁶ previously indicated a mean hop velocity of $1.2 \pm 0.2 \text{ m.s}^{-1}$ for
127 pebbles in an annular flume. This modal lap duration of $\sim 3 \text{ s}$ therefore represents a continuous
128 succession of hops over a full lap, without any resting time. These modal values decrease
129 slightly with increasing density (Figure 4A), as expected from the larger inertial effects after
130 the pebble is set in motion. More importantly, they are almost independent of the pebble shape,
131 as was also observed in a straight flume study⁶³. This implies that the impact of shape on the
132 mean traveled distance is mostly caused by its influence on the resting time between
133 movements, i.e. on the immobilization conditions and on the threshold for setting pebbles in
134 motion. To illustrate this inference, a simple calculation of the mean resting time fraction, or
135 immobility ratio (I_r), can be estimated through

$$I_r = \frac{T - N_l t_m}{T} \quad , \quad \text{Equation (1)}$$

136
137 with T being the total duration of the runs, N_l the number of achieved flume revolutions during
138 T , and t_m the modal lap duration (first mode on the distribution of Figure 1) corresponding to a
139 continuous succession of hops over a full lap.



140
 141 **Figure 4. (A) mean hop velocity and (B) time fraction of immobility of the 16 different**
 142 **artificial pebbles.**

143 Except for spherical pebbles that display a slight increase, the immobility ratio (Figure
 144 4B) is only weakly or not affected by the particle density. In contrast, the shape of a pebble
 145 deeply impacts its mobility, with the immobility ratio raging from ~50% for the spherical
 146 shapes up to $\geq 85\%$ for the elongated blades.

147
 148 **DISCUSSION**

149 The greater velocity of the spherical and compact-blade-shaped particles relative to the
 150 elongated-blade and disc-shaped particles is in good accordance with the literature^{1,39,64}, given
 151 that the flatness of the flume bottom constitutes a low roughness bed surface, despite clustering
 152 of temporary resting pebbles. As most lithologies of the pebbles present in rivers show a density
 153 close to 2.7 g.cm^{-3} , very similar to the highest value used in this study, we expect their mean
 154 velocities to be more strongly influenced by their shape than by their density. On a quantitative
 155 basis, this supports the claimed need to include a particle shape parameter in the sediment
 156 transport equation^{34,41,65}.

157 To do this, we focus on the conditions for setting a particle in motion, because pebble
 158 shape has a major influence on virtual velocity through resting periods. Following Komar and

159 Li's (1986)⁴¹ description, balancing of the moments of tractive and resisting forces for the
 160 critical stress yields:

$$161 \quad \tau_c \propto \frac{l_w \Delta \rho g S I L}{l_D A_a} \quad \text{Equation (2)}$$

162 where A_a is the apparent section exposed to the flow, and l_D and l_w the respective moment
 163 arms of the drag force and submerged weight respectively. Assuming that pebbles tend to lie
 164 with their S -axis vertically oriented, the moment arms of the drag force l_D approximately scales
 165 with the S -axis. As a pebble can orient either longitudinally or transversally, we use the
 166 intermediate variable \sqrt{LI} to account for the apparent section exposed to the flow ($A_a \propto S\sqrt{LI}$)
 167 and the moment arm of the submerged weight l_w . Therefore:

$$168 \quad \tau_c \cong k \frac{\sqrt{LI} \Delta \rho g^3 \sqrt{(SIL)^2 \tilde{D}}}{S^2 \sqrt{LI}} = k^3 \sqrt{\frac{(LI)^2}{S^4}} \Delta \rho g \tilde{D} = k \frac{1}{\Psi_p^2} \Delta \rho g \tilde{D} \quad \text{Equation (3)}$$

169 where k is a function of the particles' Reynold number considered as a constant, $\tilde{D} =$
 170 $\sqrt[3]{SIL}$, the mean pebble size, and $\Psi_p = \sqrt[3]{\frac{S^2}{IL}}$, the Sneed and Folk's index. Here, $\frac{1}{\Psi_p^2}$ corresponds
 171 more or less to the term $\tan \phi$ in Komar and Li (1986): when particle flatness increases (i.e.
 172 Ψ_p decreases), the pivoting angle increases and mobility is reduced. Suppressing the unknown
 173 k , the threshold can be expressed as:

$$174 \quad \tau_c \cong \left(\frac{\Delta \rho}{\Delta \rho_{ref}} \right) \left(\frac{\Psi_{P_{ref}}}{\Psi_p} \right)^2 \tau_{c_{ref}} \quad \text{Equation (4)}$$

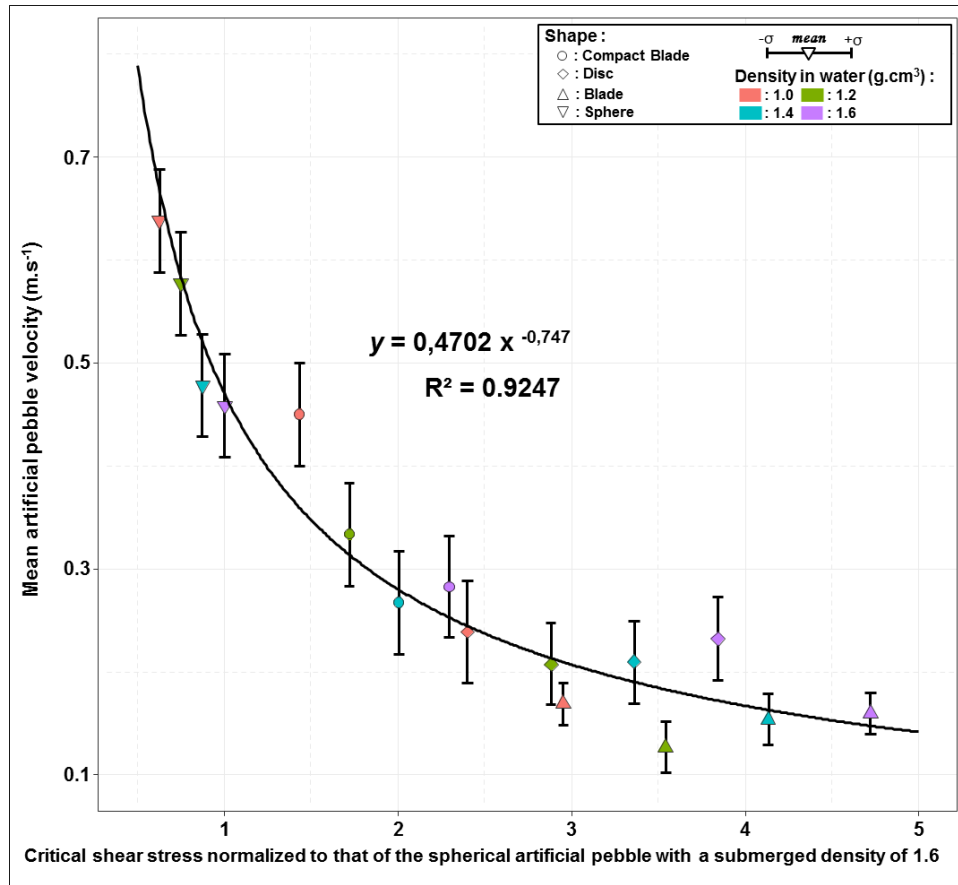
175 where $\tau_{c_{ref}}$ is the critical Shields stress of a reference pebble of similar size.

176 The non-dimensional critical threshold is expressed as:

$$177 \quad \tau_c^* \cong \frac{\tau_c}{\Delta \rho g \tilde{D}} = \frac{k}{\Psi_p^2} = \left(\frac{\Psi_{P_{ref}}}{\Psi_p} \right)^2 \tau_{c_{ref}}^* \quad \text{Equation (5)}$$

178 where $\tau_{c_{ref}}^*$ is the critical Shields stress of a reference pebble of similar size.

179 Representing the mean travel velocity of the particle as a function of the critical stress
 180 τ_c shows an inverse trend between the two variables (Figure 5): both density and departure from
 181 sphericity decrease the ratio of tractive over resistive moments and favor particle immobility.



182
 183 **Figure 5. Mean velocity of the 16 artificial pebbles vs. their critical shear stress normalized**
 184 **to that of the spherical artificial pebble with a submerged density of 1.6** ($= \frac{\tau_c}{\tau_{c_{ref}}} = \left(\frac{\Delta\rho}{1.6}\right) \left(\frac{1}{\Psi_P}\right)^2$).

185 Most bedload transport capacity formulae are functions of the excess Shields stress and
 186 follow two general forms: (1) $\Phi = K(\tau^* - \tau_c^*)^\alpha$, and (2) $W^* = (\tau/\tau_c)^\alpha$, where Φ and W^* are two
 187 distinct non-dimensional expressions of the bedload transport rate, and α and K two constant
 188 terms⁶⁶. To account for the role of pebble shape in a transport capacity relationship, one could
 189 introduce into the formula the modified expression for critical shear stress (eq. 4), or the critical
 190 Shields stress (eq. 5) that includes the Sneed and Folk Index.

191 To explore this hypothesis, we built on the fractional transport rate model developed for
 192 transport of a mixture of grain sizes (e.g. Parker et al., 1982⁶⁷). This choice was motivated by
 193 the fact that such a relation already proposes a similarity collapse for heterogeneous sediment,
 194 which is the case in our experiments with particles of variable shapes and densities mixed with
 195 a natural pebble load. We arbitrarily considered Wilcock and Crowe's (2003)⁶⁸ relation for
 196 fractional transport rate, in which the form of the similarity collapse is:

$$197 \quad W_i^* = 14 \left(1 - \frac{0.894}{\phi^{0.5}} \right)^{4.5} \quad \text{when } \phi = \frac{\tau}{\tau_{ci}} \geq 1.35 \quad \text{Equation (6)}$$

198 where τ is the bed shear stress, τ_{ci} the critical shear stress for incipient motion of a specific
 199 pebble i (more exactly it corresponds to the minimum shear stress required to achieve a small
 200 reference transport rate of $W_i^* = 0.002$ ⁶⁷), and W_i^* the dimensionless transport rate $W_i^* =$
 201 $\frac{Rgq_{bi}}{F_i \left(\frac{\tau}{\rho} \right)^{3/2}}$, with $R_i = \frac{\Delta\rho_i}{\rho}$ being the ratio of the submerged sediment (of type i) density to water
 202 density, g being gravity, q_{bi} the volumetric transport rate per unit width of the particle of type i
 203 (i.e. of similar shape, size, and density), and F_i the proportion of the pebble type being of the
 204 class i .

205 Following our simplified analysis of the force moment balance, we defined the critical
 206 (or reference) shear stress as a function (eq. 7) of the mean characteristics of the transported
 207 sediment load (i.e. mean gravel size D_m , mean shape factor Ψ_{Pm} , and mean density $\Delta\rho_m$)
 208 according to:

$$209 \quad \tau_{ci} = \left(\frac{\Delta\rho_i}{\Delta\rho_m} \right) \left(\frac{\Psi_{Pm}}{\Psi_{Pi}} \right)^2 \tau_{cm} \quad \text{Equation (7)}$$

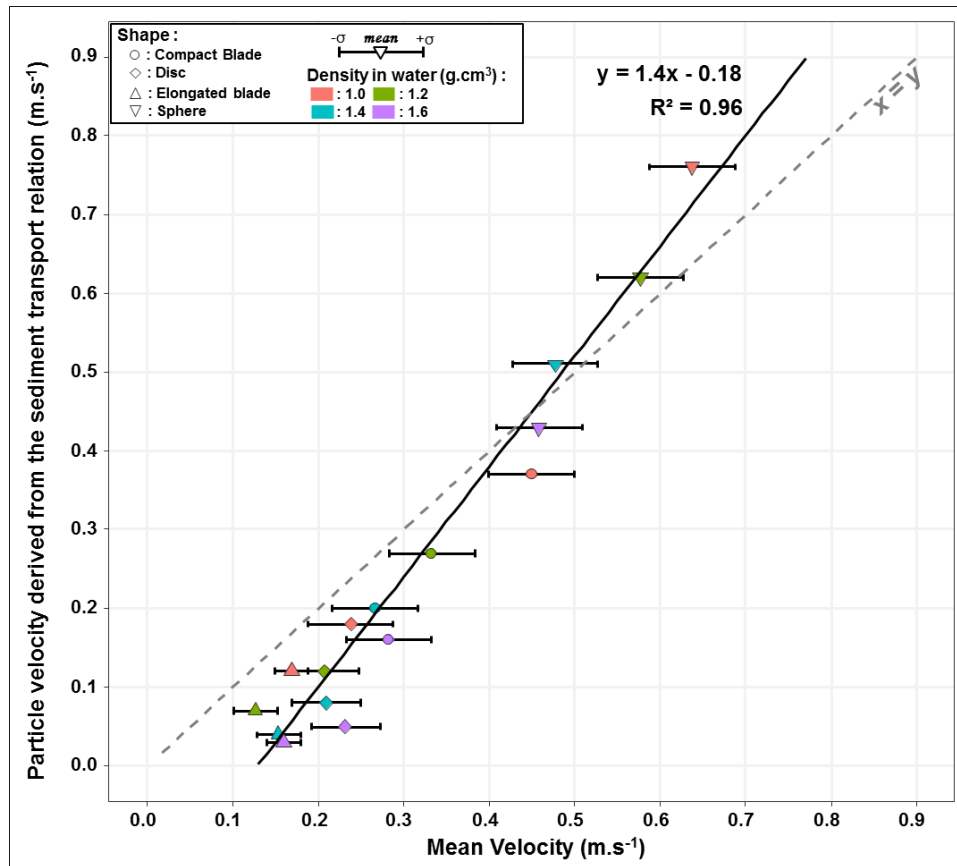
210 with τ_{cm} being the critical shear stress for the mean gravel load. Here,
 211 $\tau_{cm} = \Delta\rho_m g D_m \tau_c^* \cong 28 \text{ Pa}$ considering that $\Delta\rho = 2600 \text{ kg.m}^{-3}$, $D_m \approx 5 \text{ cm}$ for the mean
 212 gravel diameter of the 65 kg of limestone pebbles, and $\tau_c^* \cong 0.036$ ⁶⁸.

213 Within the flume, provided that not all of the particles are in full motion, the conditions
 214 of alluvial rivers prevail, i.e. the sediment flux q_{si} is equated by the transport capacity q_{bi} . In our
 215 experiments, the mass sediment flux per unit width of the pebble class i can be expressed from
 216 the mean traveling velocity through: $q_{si} = \frac{F_i M}{A} V_{gi}$, with A being the surface of the flume
 217 bottom, M the mass of sediment introduced into the flume, and V_{gi} the mean displacement
 218 velocity of particles of type i . It follows that a virtual mean velocity can be derived for particle
 219 i from the above fractional transport rate equation:

$$220 \quad V_{gi} = \frac{AM\rho_{si}}{R_i g} \left(\frac{\tau}{\rho}\right)^{3/2} W_i^* \left(\frac{\tau}{\tau_{ci}}\right) \quad \text{Equation (8)}$$

221 with τ_{ci} derived from equation (7) and a mean shape factor $\Psi_{pm} = 0.7 \pm -0.08$ for the 65 kg
 222 of limestone pebbles.

223 The virtual velocities derived from the bedload transport relation show a well-defined
 224 correlation with the measured virtual velocities (Figure 6). However, the slope of the correlation
 225 line is larger than unity, and our modified version of the bedload transport tends to
 226 underestimate the observed transport for the densest elongated-blade or disk-shaped pebbles.
 227 Despite these slight discrepancies from the observations, these results suggest that the role of
 228 pebble shape on bedload transport can be predicted, and that the inclusion of pebble shape
 229 characteristics in the modelling of bedload transport offer much promise for improving bedload
 230 transport predictions.



231

232 **Figure 6. Comparison between the mean measured velocities of particles of various shapes**
 233 **and densities and the theoretical particle velocity derived from a fractional transport rate**
 234 **relation adapted from Wilcock and Crowe’s (2003) relation ⁶⁸.**

235

236

237

238

239

240

241

242

243

244

In terms of sediment dynamics, pebbles travel in the flume following an alternating pattern of resting and motion periods, as generally observed in a natural stream⁸. We therefore consider that our experiments succeeded in capturing the first order behavior of the bedload, and that the introduction of a shape factor into critical Shield stress and bedload transport models might be transposed to rivers. However, the experimental conditions are slightly distinct from those of natural rivers, in particular the use of a monodispersed sediment load and a low-roughness bottom. Additional experiments exploring distinct bottom conditions, grain size distributions, and using straight channels are probably necessary to strengthen our initial results and resolve the slight discrepancies between the model and observations. Similarly, experiments using pebbles with a unique and defined type of particle shape (for example, only

245 platy particles, as expected in sediment derived from the erosion of schist-rich lithologies),
246 instead of a single particle mixed with a large population of pebbles of distinct shapes, should
247 help to derive a more universal relationship. Nevertheless, this study represents a preliminary
248 and promising step towards addressing the role of particle shape in bedload transport.

249

250 **CONCLUSION**

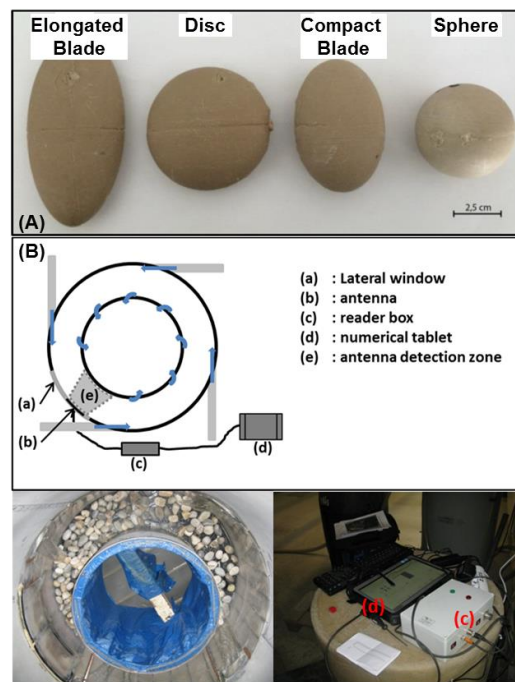
251 These experiments, based on innovative tools (artificial pebbles of controlled density
252 containing RFIDs) offer new perspectives for studying sediment transport mechanisms. The
253 comparative analysis of the shape and density of particles on their mobility highlights the
254 crucial influence of particle shape. Furthermore, it also indicates that the sphericity index (Ψ_p)
255 of Sneed and Folks (1958)⁶⁹, which correlates with mean velocity, is relevant for including
256 shape parameters in sediment transport formulae. The method developed in this study can be
257 reproduced to investigate how bed roughness (changing D/K ratio) and/or a tracer's grain-size
258 can change the balance between the effects of shape and density on particle velocity. It allows
259 investigation of whether bed roughness promotes the transport of flat-shaped particles, as
260 reported in the literature, and whether particle density can mitigate this effect. Repeating the
261 experiments with smaller particle sizes (maintaining a constant D/K ratio) would also allow
262 investigation of whether size mitigates the influence of shape and density on particle transport.

263

264 **METHODS**

265 We designed four differently-shaped particle models within the grain-size class of 45–
266 64 mm (5.5–6.0 Ψ -units), with all models having the same volume (*i.e.* 49.3 cm³) but exhibiting
267 differences in the sphericity index ⁵³ (Figure 7A ; Table 1). After creating silicon molds (RTV
268 120) for these four models, we manufactured 16 artificial pebbles using a mixture of resin and
269 corundum powder in variable proportions, creating pebbles of four different densities (2.0, 2.2,

270 2.4, and 2.6 g.cm⁻³) for each mold shape ⁵⁴. We equipped these artificial pebbles with
 271 transponders of Radio Frequency Identification, RFID, (model RI-TRP-WR2B of Texas
 272 Instrument, Dallas Texas USA, also known as PIT Tags) to monitor their displacements within
 273 an annular flume⁵⁵ (Figure 7B). A detection antenna located on the outside of the flume, along
 274 a lateral window, enabled tracking of the number of laps achieved by the RFID-equipped
 275 pebbles and the time for each revolution.



276
 277 *Figure 7. The four particle shapes investigated (A) and the*
 278 *annular flume equipped with the RFID system (B).*
 279

280 **Table 1. Shape characteristics of the artificial particles tracked in the flume.**

SHAPE	<i>a</i> -axis (mm) <i>L</i>	<i>b</i> -axis (mm) <i>I</i>	<i>c</i> -axis (mm) <i>S</i>	Vol.(cm ³)	Sphericity index (Sneed and Folks, 1958)
Compact Blade	68.1	46	30	49.3	0.66
Sphere	45.5	45.5	45.5	49.3	1
Disc	65	63	23	49.3	0.51
Elongated Blade	97.2	46.1	21	49.3	0.46

281

282 In an attempt to reproduce bedload transport conditions, these artificial pebbles were
283 mixed with 65 kg of limestone pebbles of a similar grain-size (i.e. class 45–64 mm) and were
284 run within an annular flume⁵⁶. A set of experiments were run following the designs of previous
285 studies^{54,56,57} for which the sediment dynamics have been characterized⁵⁶, i.e. with a low
286 roughness bottom and a monodispersed grain size distribution. During the experiments, the
287 pump discharge sustaining the fluid injection into the flume was maintained at 240 m³.h⁻¹,
288 which for the introduced sediment mass corresponds⁵⁶ to a shear stress of $\tau = 135$ Pa at the base
289 of the flume according to Euler theorem applied to the moments, a Shield stress of $\tau^* = 0.16$, a
290 mean transit velocity for pebbles of ≈ 0.4 m.s⁻¹, and a sediment flux of ~ 24 kg.m⁻¹.s⁻¹. Under
291 these conditions, high speed camera viewing⁵⁶ indicated that the pebbles were transported in
292 the annular flume in a similar manner to that observed⁸ in rivers, with alternating transport
293 phases with rolling and saltation, and resting times caused by temporary blockage and piling of
294 particles.

295 Each experimental run lasted for 45 minutes. To avoid superpositioning of radio-
296 frequency signals and missed RFID transponder detections^{54,58,59}, only the four particles of the
297 same density were simultaneously present in the flume, thereby also limiting to four the number
298 of transponders. A total of six runs were achieved for the densities of 2.6 and 2.4 g.cm⁻³, and
299 five runs for the densities of 2.0 and 2.2 g.cm⁻³. For each artificial pebble, the combined runs
300 provide a long duration of almost 4 hours and a large cumulative traveled distance, from which
301 the mean traveled velocity (or virtual velocity as defined by Haschenburger and Church⁶⁰) can
302 be computed and the distributions of the lap times estimated. Finally, we compared the virtual
303 velocities and lap distributions of the 16 artificial pebbles, to investigate the effects of the
304 different shapes and densities on bedload transport. In this study, the use of an annular flume
305 enabled the acquisition of a relatively long time series compared with typical straight flume
306 experiments⁶¹ and the sampling of a population of practically uncensored particle trajectories

307 without the limitations induced by a limited detection window or flume length⁶². This ensured
308 that the ranges of traveled distances under conditions of continuous movement were well
309 represented in the experiment. We also made sure that the duration of the experiments (45
310 minutes) was much longer than the maximum resting time recorded (~5 minutes), to avoid time
311 censorship effects on the distributions of the resting periods and lap times, and to be sure of the
312 statistical significance of the distributions.

313

314

315

316

317

318

319

320

321

322

323

324

325

326

327

328

329

330

331

332 **References:**

- 333 1. Demir, T. & Walsh, R. P. D. Shape and size characteristics of bedload transported during winter
334 storm events in the Cwm Treweryn Stream, Brecon Beacons, South Wales. *Turk. J. Earth Sci.* **14**,
335 105–121 (2005).
- 336 2. Mears, A. I. Flooding and sediment transport in a small alpine drainage basin in Colorado.
337 *Geology* **7**, 53 (1979).
- 338 3. Bradley, W. C. & Mears, A. I. Calculations of Flows Needed to Transport Coarse Fraction of
339 Boulder Creek Alluvium at Boulder, Colorado. *Geol. Soc. Am. Bull.* **91**, 1057–1090 (1980).
- 340 4. Einstein, H. A. & El-Samni, E.-S. A. Hydrodynamic Forces on a Rough Wall. *Rev. Mod. Phys.* **21**,
341 520–524 (1949).
- 342 5. Cheng, E. D. H. & Clyde, C. G. Instantaneous hydrodynamic lift and drag forces on large
343 roughness elements in turbulent open channel flow. in 3-1-3–20 (H. W. Shen, 1972).
- 344 6. Komar, P. D. & Li, Z. Applications of grain-pivoting and sliding analyses to selective entrapment of
345 gravel and to flow-competence evaluations. *Sedimentology* **35**, 681–695 (1988).
- 346 7. Einstein, H. Bed load transport as a probability problem. 1–105 (1937).
- 347 8. Habersack, H. M. Radio-tracking gravel particles in a large braided river in New Zealand: A field
348 test of the stochastic theory of bed load transport proposed by Einstein. *Hydrol. Process.* **15**,
349 377–391 (2001).
- 350 9. Olinde, L. & Johnson, J. Using RFID and accelerometer-embedded tracers to measure
351 probabilities of bed load transport, step lengths, and rest times in a mountain stream. *Water*
352 *Resour Res* **51**, 7572–7589 (2015).
- 353 10. Hjulström, F. Studies of the morphological activity of rivers as illustrated by the River Fyris.
354 Inaugural dissertation,. (Almqvist & Wiksells, 1935).
- 355 11. Einstein, A. H. Bedload transport as a probability problem. (Colorado State University, 1937).

- 356 12. Ergenzinger, P. & Schmidt, K. H. Stochastic elements of bed load transport in a steppool
357 mountain river. *Hydrol. Mt. Reg. II—Artificial Reserv. Water Slopes Int. Assoc. Hydrol. Sci. Publ.*
358 **194**, 39–46 (1990).
- 359 13. Busskamp, R. The influence of channel steps on coarse bed load transport in mountain torrents:
360 case study using the radio tracer technique ‘PETSU’. in *Dynamics and geomorphology of*
361 *mountain rivers* 129–139 (Springer, 1994).
- 362 14. Olinde, L. Displacement and entrainment behavior of bedload clasts in mountain streams.
363 (University of Texas, 2015).
- 364 15. Shields, A. Application of similarity principles and turbulence research to bed-load movement.
365 *CalTech Libr.* (1936).
- 366 16. Meyer-Peter, E. & Müller, R. Formulas for Bed-Load transport. *IAHSR 2nd Meet. Stockh. Append.*
367 **2** (1948).
- 368 17. Engelund, F. & Hansen, E. A monograph on sediment transport in alluvial streams. *Tech. Univ.*
369 *Den. Ostervoldgade 10 Cph. K* (1967).
- 370 18. Ackers, P. & White, W. R. Sediment Transport: New Approach and Analysis. *J. Hydraul. Div.* **99**,
371 2041–2060 (1973).
- 372 19. Parker, G. & Klingeman, P. C. On why gravel bed streams are paved. *Water Resour. Res.* **18**,
373 1409–1423 (1982).
- 374 20. Recking, A., Frey, P., Paquier, A., Belleudy, P. & Champagne, J. Y. Feedback between bed load
375 transport and flow resistance in gravel and cobble bed rivers: FEEDBACK BETWEEN BED LOAD
376 AND FLOW RESISTANCE. *Water Resour. Res.* **44**, (2008).
- 377 21. Piton, G. & Recking, A. The concept of travelling bedload and its consequences for bedload
378 computation in mountain streams: HOW TO ACCOUNT FOR ALLOGENIC SUPPLY IN BEDLOAD
379 TRANSPORT EQUATIONS? *Earth Surf. Process. Landf.* (2017) doi:10.1002/esp.4105.
- 380 22. Rickenmann, D. Hyperconcentrated Flow and Sediment Transport at Steep Slopes. *J. Hydraul.*
381 *Eng.* **117**, 1419–1439 (1991).

- 382 23. Smart, G. & Jäggi, M. *Sediment transport on steep slopes. Mitteilung. 64. Versuchsanstalt für*
383 *Wasserbau, Hydrologie und Glaziologie.* (ETH Zurich, Zurich, 1983).
- 384 24. Parker, G., Klingeman, P. C. & McLean, D. G. Bedload and Size Distribution in Paved Gravel-Bed
385 Streams. *J. Hydraul. Div.* **108**, 544–571 (1982).
- 386 25. Wilcock, P. R. & Crowe, J. C. Surface-based Transport Model for Mixed-Size Sediment. *J. Hydraul.*
387 *Eng.* **129**, 120–128 (2003).
- 388 26. van Rijn, L. C. Sediment Transport, Part I: Bed Load Transport. *J. Hydraul. Eng.* **110**, 1431–1456
389 (1984).
- 390 27. Recking, A. Theoretical development on the effects of changing flow hydraulics on incipient bed
391 load motion: INCIPIENT MOTION CONDITIONS. *Water Resour. Res.* **45**, (2009).
- 392 28. Frey, P. & Church, M. How River Beds Move. *Science* **325**, 1509–1510 (2009).
- 393 29. Buffington, J. M. & Montgomery, D. R. A systematic analysis of eight decades of incipient motion
394 studies, with special reference to gravel-bedded rivers. *Water Resour. Res.* **33**, 1993–2029
395 (1997).
- 396 30. Gessler, J. *Chapter 7 Preprint of Paper Beginning and Ceasing of Sediment Motion.* (Colorado
397 State University, 1970).
- 398 31. Miller, M. C., McCAYE, I. N. & Komar, P. D. Threshold of sediment motion under unidirectional
399 currents. *Sedimentology* **24**, 507–527 (1977).
- 400 32. Yalin, M. S. & Silva, A. M. F. da. *Fluvial processes.* (IAHR, 2001).
- 401 33. Miller, R. L. & Byrne, R. J. The angle of repose for a single grain on a fixed rough bed.
402 *Sedimentology* **6**, 303–314 (1966).
- 403 34. Li, Z. & Komar, P. D. Laboratory measurements of pivoting angles for applications to selective
404 entrainment of gravel in a current. *Sedimentology* **33**, 413–423 (1986).
- 405 35. Kirchner, J. W., Dietrich, W. E., Iseya, F. & Ikeda, H. The variability of critical shear stress, friction
406 angle, and grain protrusion in water-worked sediments. *Sedimentology* **37**, 647–672 (1990).

- 407 36. Buffington, J. M., Dietrich, W. E. & Kirchner, J. W. Friction angle measurements on a naturally
408 formed gravel streambed: Implications for critical boundary shear stress. *Water Resour. Res.* **28**,
409 411–425 (1992).
- 410 37. Lamb, M. P., Brun, F. & Fuller, B. M. Hydrodynamics of steep streams with planar coarse-grained
411 beds: Turbulence, flow resistance, and implications for sediment transport: HYDRODYNAMICS OF
412 STEEP STREAMS. *Water Resour. Res.* **53**, 2240–2263 (2017).
- 413 38. Miller, R. L. & Byrne, R. J. The Angle of Repose for a Single Grain on a Fixed Rough Bed.
414 *Sedimentology* **6**, 303–314 (1966).
- 415 39. Carling, P. A., Kelsey, A. & Glaister, M. S. Effect of bed roughness, particle shape and orientation
416 on initial motion criteria. in *Dynamics of Gravel-bed Rivers* 24–39 (Hey, R.D. Billi, P., Thorne, C.R.
417 and Tacconi, P. (eds), 1992).
- 418 40. Lane, E. W. & Carlson, E. J. Some observations on the effect of particle shape on the movement
419 of coarse sediments. *Eos Trans. Am. Geophys. Union* **35**, 453–462 (1954).
- 420 41. Komar, P. D. & Li, Z. Pivoting analyses of the selective entrainment of sediments by shape and
421 size with application to gravel threshold. *Sedimentology* **33**, 425–436 (1986).
- 422 42. Schmidt, K.-H. & Ergenzinger, P. Bedload entrainment, travel lengths, step lengths, rest periods—
423 studied with passive (iron, magnetic) and active (radio) tracer techniques. *Earth Surf. Process.*
424 *Landf.* **17**, 147–165 (1992).
- 425 43. Schmidt, K.-H. & Gintz, D. Results of Bed load tracer experiments in a mountain river. in *River*
426 *Geomorphology* 37–54 (Wiley, 1995).
- 427 44. Buffington, J. M., Dietrich, W. E. & Kirchner, J. W. Friction angle measurements on a naturally
428 formed gravel streambed: Implications for critical boundary shear stress. *Water Resour. Res.* **28**,
429 411–425 (1992).
- 430 45. White, C. M. The Equilibrium of Grains on the Bed of a Stream. *Proc. R. Soc. Math. Phys. Eng. Sci.*
431 **174**, 322–338 (1940).
- 432 46. Zingg, T. Beitrag zur Schotteranalyse. (1935).

- 433 47. Barrett, P. J. The shape of rock particles, a critical review. *Sedimentology* **27**, 291–303 (1980).
- 434 48. Blott, S. J. & Pye, K. Particle shape: a review and new methods of characterization and
435 classification. *Sedimentology* **55**, 31–63 (2008).
- 436 49. Domokos, G., Sipos, A., Szabó, T. & Várkonyi, P. Pebbles, Shapes, and Equilibria. *Math. Geosci.*
437 **42**, 29–47 (2009).
- 438 50. Szabó, T. & Domokos, G. A new classification system for pebble and crystal shapes based on
439 static equilibrium points. *Cent. Eur. Geol.* **53**, 1–19 (2010).
- 440 51. Domokos, G., Kun, F., Sipos, A. Á. & Szabó, T. Universality of fragment shapes. *Sci. Rep.* **5**, (2015).
- 441 52. Novák-Szabó, T. *et al.* Universal characteristics of particle shape evolution by bed-load chipping.
442 *Sci. Adv.* **4**, eaao4946 (2018).
- 443 53. Oakey, R. J. *et al.* Grain-Shape Analysis--A New Method for Determining Representative Particle
444 Shapes for Populations of Natural Grains. *J. Sediment. Res.* **75**, 1065–1073 (2005).
- 445 54. Cassel, M., Piégay, H. & Lavé, J. Effects of transport and insertion of radio frequency
446 identification (RFID) transponders on resistance and shape of natural and synthetic pebbles:
447 applications for riverine and coastal bedload tracking: Transport and Rfid-Insertion Effects on the
448 Fragility of Pebbles. *Earth Surf. Process. Landf.* (2016) doi:10.1002/esp.3989.
- 449 55. Attal, M., Lave, J. & Masson, J. P. New Facility to Study River Abrasion Processes. *J. Hydraul. Eng.*
450 **132**, 624–628 (2006).
- 451 56. Attal, M. & Lavé, J. Pebble abrasion during fluvial transport: Experimental results and
452 implications for the evolution of the sediment load along rivers. *J. Geophys. Res.* **114**, (2009).
- 453 57. Cassel, M. *et al.* Evaluating a 2D image-based computerized approach for measuring riverine
454 pebble roundness. *Geomorphology* (2018) doi:10.1016/j.geomorph.2018.03.020.
- 455 58. Chapuis, M., Bright, C. J., Hufnagel, J. & MacVicar, B. Detection ranges and uncertainty of passive
456 Radio Frequency Identification (RFID) transponders for sediment tracking in gravel rivers and
457 coastal environments. *Earth Surf. Process. Landf.* **39**, 2109–2120 (2014).

- 458 59. Arnaud, F., Piégay, H., Vaudor, L., Bultingaire, L. & Fantino, G. Technical specifications of low-
459 frequency radio identification bedload tracking from field experiments: Differences in antennas,
460 tags and operators. *Geomorphology* **238**, 37–46 (2015).
- 461 60. Haschenburger, J. K. & Church, M. Bed material transport estimated from the virtual velocity of
462 sediment. *Earth Surf. Process. Landf.* **23**, 791–808 (1998).
- 463 61. Cecchetto, M. *et al.* Diffusive Regimes of the Motion of Bed Load Particles in Open Channel Flows
464 at Low Transport Stages. *Water Resour. Res.* **54**, 8674–8691 (2018).
- 465 62. Ballio, F., Radice, A., Fathel, S. L. & Furbish, D. J. Experimental Censorship of Bed Load Particle
466 Motions and Bias Correction of the Associated Frequency Distributions. *J. Geophys. Res. Earth*
467 *Surf.* **124**, 116–136 (2019).
- 468 63. Auel, C., Albayrak, I., Sumi, T. & Boes, R. M. Sediment transport in high-speed flows over a fixed
469 bed: 1. Particle dynamics. *Earth Surf. Process. Landf.* **42**, 1365–1383 (2017).
- 470 64. Demir, T. The influence of particle shape on bedload transport in coarse-bed river channels.
471 (Durham University, 2000).
- 472 65. Bridge, J. S. & Bennett, S. J. A model for the entrainment and transport of sediment grains of
473 mixed sizes, shapes, and densities. *Water Resour. Res.* **28**, 337–363 (1992).
- 474 66. Bagnold, R. A. *An approach to the sediment transport problem from general physics.*
475 <http://pubs.er.usgs.gov/publication/pp4221> (1966).
- 476 67. Parker, G., Klingeman, P. C. & McLean, D. G. BEDLOAD AND SIZE DISTRIBUTION IN PAVED
477 GRAVEL-BED STREAMS. *ASCE J Hydraul Div* **108**, 544–571 (1982).
- 478 68. Wilcock, P. R. & Crowe, J. C. Surface-based Transport Model for Mixed-Size Sediment. *J. Hydraul.*
479 *Eng.* **129**, 120–128 (2003).
- 480 69. Sneed, E. D. & Folk, R. L. Pebbles in the Lower Colorado River, Texas a Study in Particle
481 Morphogenesis. *J. Geol.* **66**, 114–150 (1958).

482

483

484 **Author contributions**

485 M.C., H.P., and J.L. contributed to the design of the experiment. M.C., J.L., and H.P. analyzed
486 experimental results; J.L., H.P., M.C., A.R., and J-R.M. wrote the manuscript.

487

488 **Corresponding author**

489 Correspondence to Mathieu Cassel.

490

491 **Competing Interests**

492 The authors declare no competing interests.